3D numerical simulation of the supersonic combustion of H_2

Prashant Dinde, A. Rajasekaran and V. Babu
Department of Mechanical Engineering
Indian Institute of Technology
Madras, India

ABSTRACT

Results from numerical simulations of supersonic combustion of H_2 are presented. The combustor has a single stage fuel injection parallel to the main flow from the base of a wedge. The simulations have been performed using FLUENT. Realisable k-ε model has been used for modelling turbulence and single step finite rate chemistry has been used for modelling the H_2-Air kinetics. All the numerical solutions have been obtained on grids with average value for wall y+ less than 40. Numerically predicted profiles of static pressure, axial velocity, turbulent kinetic energy and static temperature for both non-reacting as well as reacting flows are compared with the experimental data. The RANS calculations are able to predict the mean and fluctuating quantities reasonably well in most regions of the flow field. However, the single step kinetics predicts heat release much more rapid than what was seen in the experiments. Nonetheless, the overall pressure rise in the combustor due to combustion is predicted well. Also, the k-ε model is not able to predict the fluctuating quantities in the base region of the wedge where there is strong anisotropy in the presence of combustion.

NOMENCLATURE

A	cross-sectional area
k	turbulent kinetic energy
$m_{fuel,in}$	mass flow rate of fuel
Ma	Mach number
P	static pressure
P_0	local stagnation pressure
$P_{0,inlet}$	inlet stagnation pressure
T	static temperature
T_0	local stagnation temperature
$T_{0,inlet}$	inlet stagnation temperature
u	velocity along the x-direction
Y_i	mass fraction of species i

Greek symbols

α	local fuel mass fraction
α_s	stoichiometric fuel mass fraction
ε	turbulent strain rate
η_c	combustion efficiency

Paper No. 3047. Manuscript received 1 December 2005, revised paper received 4 September 2006, accepted 18 October 2006.

https://doi.org/10.1017/S0001924000001640 Published online by Cambridge University Press

η_m mixing efficiency
η_t total pressure loss
ρ mass density

Abbreviations

RANS Reynolds Averaged Navier Stokes
SST Shear Stress Transport
LES Large Eddy Simulation

1.0 INTRODUCTION

There is renewed interest in scramjet technology in recent years and the successful third test flight of the NASA X-23 hypersonic propulsion vehicle attests to the technical feasibility of this technology. It is well known that a crucial element in the successful development of hypersonic propulsion device is an efficient supersonic combustor. The supersonic flow conditions in the combustor lead to very short residence times for the fuel and air, typically of the order of a few milliseconds. The fuel has to mix with the supersonic flow and burn completely within such a short duration of time. The ignition and reaction times of the fuel, therefore, have to be short. Hydrogen is ideally suited to meet these requirements. During the course of the development of a viable supersonic combustor, extensive experimental investigations of model combustors with different injection and flame stabilisation techniques have been carried out. In contrast, fully resolved, numerical simulations of the 3D, turbulent, reacting flow in the supersonic combustor are limited. This provides the motivation for the present work. A brief review of the available literature on numerical simulations of supersonic combustion is given below.

Goyne *et al*[1], carried out numerical simulations of H_2 combustion in a supersonic air flow with hydrogen injection parallel to the air stream. The flow was modelled as chemically reacting mixture of thermally perfect gases. A single step four species chemistry model was used. Numerical predictions agreed well with the experimental data for the fuel-off and mixing cases. However, for reacting flow, the model under-predicted the pressure rise due to combustion.

Kim *et al*[2], investigated the effect of shock waves on a supersonic H_2-Air jet flame stabilised in a Mach 2·5 circular combustor. A numerical model based on multi-species Navier-Stokes equations with detailed chemistry and k-ω SST model was employed. It was found that the shock waves created a radially inward/outward airflow to the flame and an elongated flame holding recirculation zone, thereby enhancing the fuel-air mixing efficiency. Upstream location of the shock wave was shown to increase the size of flame holding recirculation zone. This increased the combustion efficiency albeit with an increase in the total pressure loss.

Kim *et al*[3] carried out 2D numerical calculations of supersonic combustion with cavity based fuel injection. The effects of varying cavity aft wall angle and the cavity length on the hydrogen injection into the supersonic air flow were investigated. The cavity was found to enhance combustion efficiency but it also increased the total pressure loss.

Rodriguez *et al*[4] analysed 3D effects in dual mode scramjets. A Wilcox k-ω turbulence model along with a seven species, seven equation finite rate chemistry model was used. The numerical calculations over-predicted the peak wall pressure as well as mixing and combustion efficiencies when compared with experimental data. Rodriguez and Cutler[5] carried out 3D numerical calculations in a SCHOLAR supersonic combustor. In this combustor, Hydrogen was injected at an angle of 30° from the wall into a Mach 2·5 supersonic air stream. The numerical solutions were found to be sensitive to the type of turbulence model and the inflow turbulence parameters used. The difficulty in accurately predicting the ignition delay time, combustion pressure rise and fuel plume penetration was discussed in their paper.

Baurle[6] gave a comprehensive overview of various CFD techniques used for the modelling of high speed flows. The need for steady state RANS in solving the compressible reacting flow in high speed commercial and military application was explained in his paper. A detailed discussion of LES models currently in use and the necessity for improving compressible reacting flow models using RANS was presented. The superiority of higher order Reynolds stress tensor model over linear models currently in use, in predicting the mixing and combustion efficiency was demonstrated. The sensitivity of the predictions to parameters like turbulent Schmidt and Prandtl number was investigated in detail in this paper.

Rajasekaran and Babu[7] presented numerical results for the 3D reacting flow in a model supersonic combustor utilising strut and wall based fuel injection schemes (normal to the main flow) with H_2 fuel. Single step chemistry with one equation Spalart-Allmaras model was used for the calculations. Predicted values of wall static pressure were compared with experimental data. While the calculations could predict the overall pressure rise, pressure rise due to combustion could not be predicted well.

Oevermann[8] carried out 2D calculations of turbulent combustion using a laminar flamelet model and standard k-ε model. However, the flow was allowed to slip over wall surfaces. Comparison of the numerical predictions with experimental data was also presented. This brought out the limitations of the flamelet model.

The motivation of the present work is to address these deficiencies and determine how well 3D numerical simulations can predict the flow and temperature fields in the supersonic combustion of H_2. To this end, numerical calculations of the 3D, compressible, reacting flow with single step finite rate chemistry and realisable k-ε model on very fine meshes have been carried out using FLUENT. The geometry considered in this work is the same as the one considered by Oevermann[8]. Results from the numerical calculations for mean as well fluctuating quantities are compared with experimental data for this geometry reported by Oevermann[8]. This allows a critical evaluation to be made about the capability of CFD to predict such flows accurately.

2.0 FORMULATION AND SOLUTION METHODOLOGY

The model supersonic combustor considered in the present work is shown in Fig. 1. The combustor is 0·3m long, and 0·05m high at the inlet and 0·057m high at the exit, and the total width is 0·045m. Vitiated air enters through the inlet, with hydrogen being injected through the bottom of the wedge. The Mach number at the inlet is two and the stagnation temperature and pressure for the vitiated air are 612K and 7·825 bar respectively. Fuel is injected from the base of the wedge which is located at a distance of 0·035m from the inlet. The wedge is 0·032m long and the semi-vertex angle is 6°. The inlet conditions of the H_2 injection ports are adjusted so as to achieve sonic injection with the desired fuel mass flow rate. The equivalence ratio is 0·0125. The flow through the combustor is compressible and three-dimensional. In addition, turbulence and finite rate chemistry are also considered.

Realisable k-ε model is used for modelling turbulence with default values for the constants ($C_{1\varepsilon}$ = 1·44, $C_{2\varepsilon}$ = 1·9). The turbulent Prandtl and Schmidt numbers have been assumed to be 1·2, 0·7 respectively. Effect of changing the values for the constants in the turbulence chemistry model, especially the turbulent Schmidt number has not been investigated in the present work. In this connection, it is important to keep in mind

https://doi.org/10.1017/S0001924000001640 Published online by Cambridge University Press

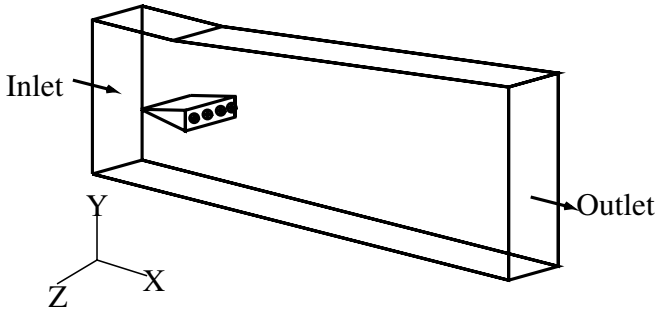


Figure 1. Geometry of the model supersonic combustor.

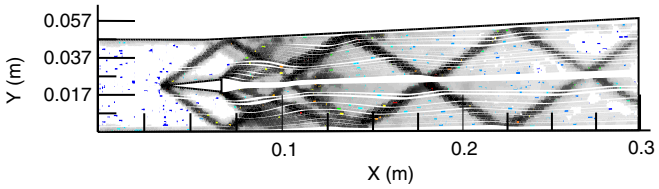


Figure 2. Path lines on the symmetry plane coloured by pressure gradient; non-reacting flow. Colour scale goes from red (high) through green (medium) to blue (low).

that the heat release and the pressure rise in the combustor are quite sensitive to the values used for turbulent Schmidt and Prandtl numbers[9]. Single step, laminar, finite rate kinetics has been used to model chemistry. Rate data for the H_2-O_2 forward reaction mechanism has been taken from Hsu and Jemcov[10]. Viscosity and C_p of the mixture have been evaluated using mass-weighted mixing law. For the individual fluids in the mixture, these properties have been evaluated using Sutherland's law and 5th order polynomials in temperature respectively.

Although the full geometry is shown in Fig. 1, calculations have been carried out in half geometry as the flowfield can be considered to be symmetric about the vertical mid-plane. Adiabatic boundary conditions with standard wall functions have been used on all the wall surfaces. At the air inlet, total and static pressure, total temperature and species mass fractions are specified. In addition, k and ε have been specified[8]. In the hydrogen injection port, mass flow inlet conditions, namely mass flow rate of hydrogen, static pressure, total temperature and species mass fractions are specified. The actual values used in these inlets are the same as those given by Oevermann[8] and these are reproduced in Table 1 for convenience. All the flow variables at the outlet boundary including pressure are determined from the interior of the domain by extrapolation, as the flow is supersonic here.

3.0 GRID INDEPENDENCE STUDY

Numerical calculations of the flow with fuel injection but without chemical reaction were first carried out on a base grid with 205,460 tetrahedral cells. The wall y+ on this grid was 134 and 129 respectively for first order and second order accurate calculations. This grid was then refined by adaption based on gradients of static pressure to capture the shocks, followed by refinement near all the no-slip surfaces to resolve the boundary layers well.

Table 1
Inflow conditions of the air stream and the hydrogen jet[8]

Condition	Air	Hydrogen
Ma	2·0	1·0
u [ms^{-1}]	730	1,200
T [K]	340	250
P [105 Pa]	1·0	1·0
ρ [kg/m^3]	1·002	0·097
YO_2	0·232	0
YN_2	0·736	0
YH_2O	0·032	0
YH_2	0	1
k [m^2/s^2]	10	2,400
ε [m^2/s^3]	650	10^8

The grid was further refined in the shear layer between the hydrogen jet and the incoming air so as to resolve the mixing and diffusion effects of hydrogen effectively. This refinement resulted in grids with 281,431 cells. The maximum value of wall y+ for the latter grid was approximately 76 for second order accurate calculations. This grid has been used for the non-reacting flow calculations. It should be noted that the gradient adaption refines the grid primarily along the flow direction and so does not change the wall y+ values. All the refinement has been done in FLUENT itself rather than in the associated mesh generation software GAMBIT.

For reacting flow calculations the grid was adapted further based on the gradients of reacting species so as to resolve the combustion phenomenon in the flow field accurately. After progressive refinement, a grid with 340,840 cells has been taken as the final grid for all subsequent calculations. The maximum value of wall y+ on this grid is 80, while the area averaged value is 37. These details are summarised in Table. 2. For turbulent calculations using standard wall functions such as the present one, wall y+ values less than 100 are generally acceptable[5]. In flows with shocks, wall y+ values tend to be high locally near the points of impingement and reflection of shocks. So the area-averaged

Table 2
Grid Independence Study

Discretization	No. of Cells	Wall y$^+$	
		Max	Avg
Non-reacting flow (no fuel)			
1st order	205460	134	79
2nd order	”	129	74
Non-reacting flow (with fuel injection)			
1st order	205460	139	80
2nd order	”	134	72
Gradient + Wall y$^+$ Adaption			
1st order	281431	79	42
2nd order	”	76	37
Gradient Adaption			
1st order	340840	81	42
2nd order	”	80	37

https://doi.org/10.1017/S0001924000001640 Published online by Cambridge University Press

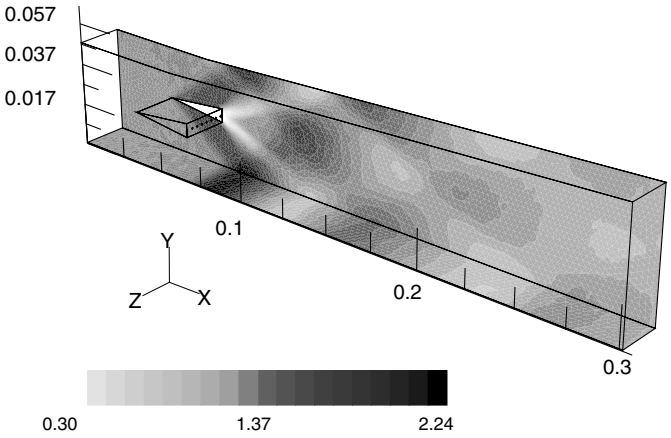


Figure 3. Contours of pressure (bar) on the side and bottom walls; non-reacting flow.

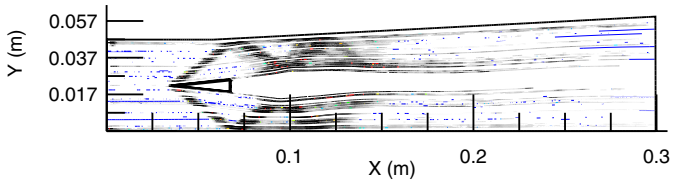


Figure 4. Path lines on the symmetry plane coloured by pressure gradient; reacting flow. Colour scale goes from red (high) through green (medium) to blue (low).

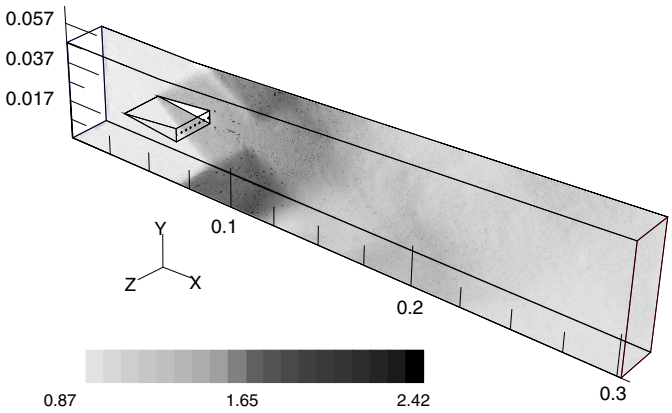


Figure 5. Contours of pressure (bar) on the side and bottom walls; reacting flow.

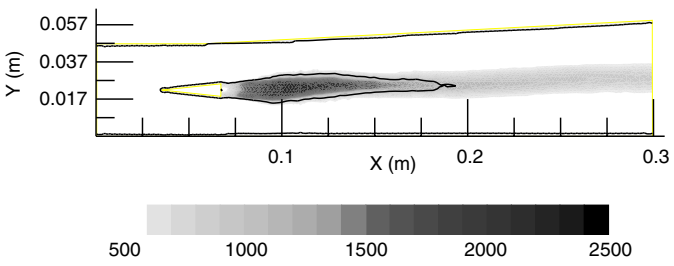


Figure 6. Contours of static temperature (K) on the symmetry plane; reacting flow.

wall $y+$ yields a more realistic estimate. Furthermore, global (overall) mass conservation is also important, and for all the results reported here, the difference in mass between inlet(s) and outlet is about 6×10^{-5}kg/s. This corresponds to less than 0·01% of the mass flow rate through the domain. Fuel mass conservation is about 98%

4.0 RESULTS AND DISCUSSION

4.1 Non-reacting flow

Path lines on the symmetry plane coloured by gradient of static pressure are shown in Fig. 2. The deflection of the path lines and the accompanying pressure increase/decrease clearly show the oblique shock from the leading edge of the wedge as well as the expansion fan from the trailing edge corners. This figure clearly shows the expansion fan around the corner of the wedge arising from the downward deflection of the supersonic flow. There is a recompression shock just downstream due to the straightening of the shear layer. Weak oblique shock/expansion waves generated due to the undulations in the shear layer are also visible. Multiple reflections of the shock waves from the edge of the shear layer as well as the top and bottom wall and the accompanying shock diamonds are also seen in this figure. Comparison of this figure with the Schlieren picture from the experiments[8] shows that the gradient based grid adaption used in the present calculations allows the oblique shocks/expansion fans as well as the shear layer to be captured very well.

Contours of static pressure on the side wall and the bottom wall are shown in Fig. 3. The leading–edge shock wave is reflected from the top and bottom walls but the reflected shock wave from the bottom wall is stronger compared to that from the top wall due to the 3° divergence in the latter. There is also a subsonic recirculation zone at the base of the wedge. The fuel is injected into this subsonic recirculation zone, which helps in flame stabilisation. It is interesting to see from Fig. 3 that the flow field for the non-reacting flow is only weakly three-dimensional.

4.2 Reacting flow

Path lines on the symmetry plane coloured by gradient of static pressure are shown in Fig. 4. As a result of the pressure rise due to combustion, the expansion fan around the corner of the wedge that was seen before, is totally absent now. The broadening combustion zone downstream of the wedge base till $x \approx 0{\cdot}1$m followed by a constriction is in very good agreement with the shadow picture from the experiments[8]. The minimum width of the wake occurs at $x \approx 0{\cdot}16$m which is also in good agreement with the experimental data. Oevermann[8] reported a shock at $x = 0{\cdot}18$ m, in his numerical results, but this was not seen in the experiments. The present calculations also do not show any shock at this location. The size of the combustion zone predicted by the present calculations agrees fairly well with the experimental observations.

Contours of static pressure for the reacting flow on the side and top wall are shown in Fig. 5. Comparison of this figure with Fig. 3 shows that the pressure rise due to combustion is not very high on account of the global equivalence ratio being quite low. The complete absence of the expansion around the corner of the wedge and the three-dimensionality of the flow field downstream of the wedge can be discerned from these figures. Contours of static temperature on the symmetry plane (Fig. 6) shows the combustion and heat release to be taking place in the recirculation region downstream of the wedge. The sonic line is shown

https://doi.org/10.1017/S0001924000001640 Published online by Cambridge University Press

in this figure as a thick black line. From this, it is clear that the combustion is subsonic. Since the heat addition is taking place in the divergent portion of the combustor, the flow is not thermally choked for this equivalence ratio. However, our calculations indicate that raising the equivalence ratio to 0·2 results in the formation of a normal shock just ahead of the wedge.

4.3 Overall performance measures

In this section, some 1D metrics for assessing the overall performance of the combustor, namely, mixing efficiency, combustion efficiency and loss of total pressure, are discussed. Mixing efficiency[11] indicates the extent to which the fuel and the air are in stoichiometric proportion locally. At a given x = constant section, mixing efficiency is defined as;

$$\eta_m = \frac{\int \alpha_R \rho u \mathrm{d}A}{\sum \dot{m}_{fuel,in}}$$

where, α_R is given by;

$$\alpha_R = \begin{cases} \alpha, & \alpha \le \alpha_S \\ \alpha_S \dfrac{1-\alpha}{1-\alpha_S}, & \alpha > \alpha_S \end{cases}$$

Mixing efficiency along the length of the combustor for the non-reacting flow is shown in Fig. 7. Fuel is injected from the base of the wedge at $x \approx 0{\cdot}067$m and the mixing is complete at $x \approx 0{\cdot}085$m. An examination of the contours of mass fraction of H_2 shown in Fig. 8 also indicates mixing taking place rapidly. The rapid mixing and the high values for mixing efficiency are typical of H_2 fuel. Hydrocarbon fuels show lesser values for mixing efficiency[11]. The other reason for the mixing efficiency being so high in the present case is the low global equivalence ratio.

Combustion efficiency[11] at a given x = constant section is a measure of how much of the fuel injected upstream has been consumed at that station. This is defined as[11];

$$\eta_C = 1 - \frac{\int \alpha \rho u \mathrm{d}A}{\sum \dot{m}_{fuel,in}}$$

The plot of combustion efficiency in Fig. 7, shows that it reaches 100% asymptotically. It appears from this figure that combustion is essentially complete at $x \approx 0{\cdot}12$m. Contours of the mass fraction of H_2O are given in Fig. 9. It can be seen that the maximum value for the mass fraction of H_2O is reached at a distance of 0·08 m, which is just downstream of the base of the wedge. However, the distribution of the mass fraction of H_2O continues to change till 0·15m, beyond which it remains the same. The species mass fractions are frozen beyond this point as the flow velocity increases and the static temperature decreases due to the expansion in the divergent part. Contours of the reaction rate and static temperature on different planes downstream of the wedge shown in Figs 10 and 11 corroborate these observations. Furthermore, the effect of finite rate chemistry is brought out clearly in these figures. The reaction rate attains its maximum value in the shear layer, but the static temperature and the mass fraction of H_2O attain their maximum values inside the recirculation region. Since the velocity is quite high in the shear layer, residence time is lower. Consequently, although the rates are high, reaction is kinetically controlled in the shear layer. On the other hand, the velocity is lower inside the recirculation region and so the residence time is longer thus allowing more water vapour to be formed. Thus, the reaction is mixing controlled inside the recirculation region.

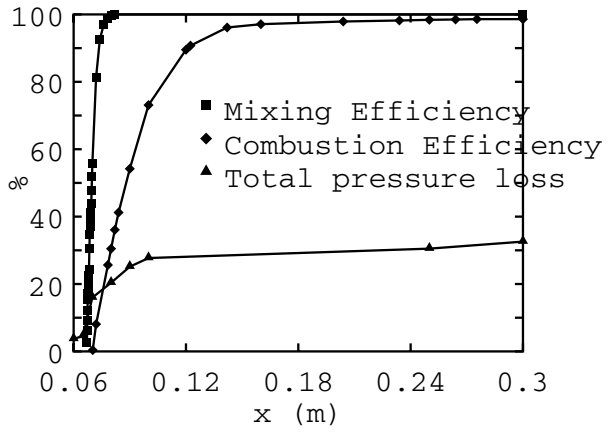


Figure 7. Variation of mixing efficiency, combustion efficiency and total pressure loss along the *x*-direction.

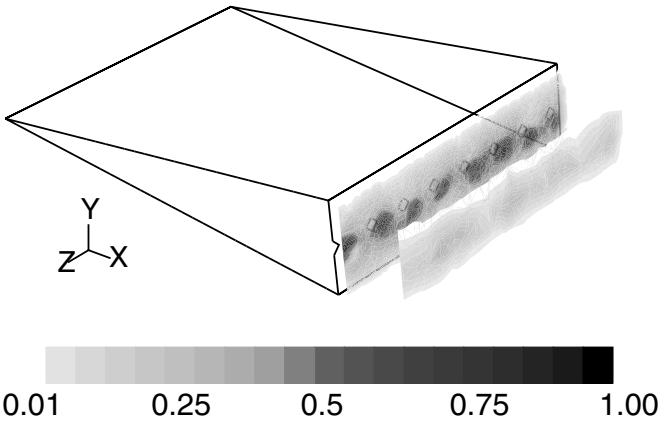


Figure 8. Contours of H_2 mass fraction; non-reacting flow.

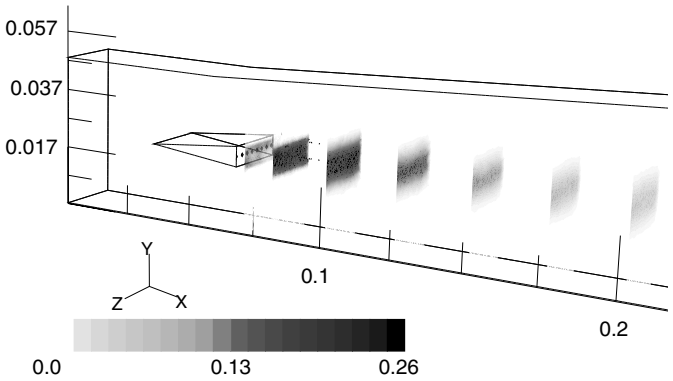


Figure 9. Contours of H_2O mass fraction; reacting flow.

https://doi.org/10.1017/S0001924000001640 Published online by Cambridge University Press

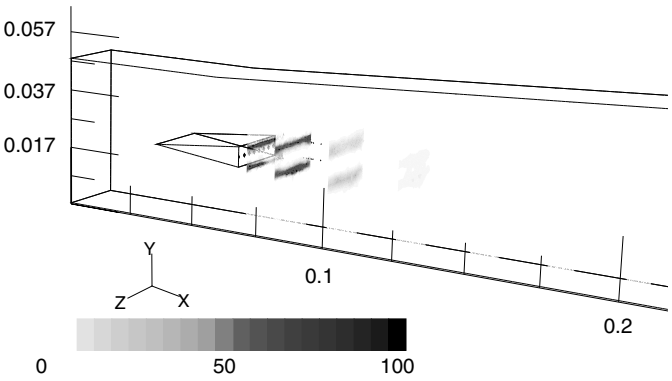


Figure 10. Contours of reaction rate ($kgmol/m^3.s$).

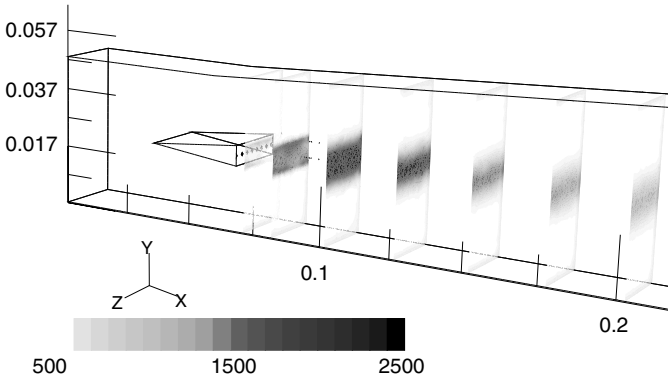


Figure 11. Contours of static temperature (K).

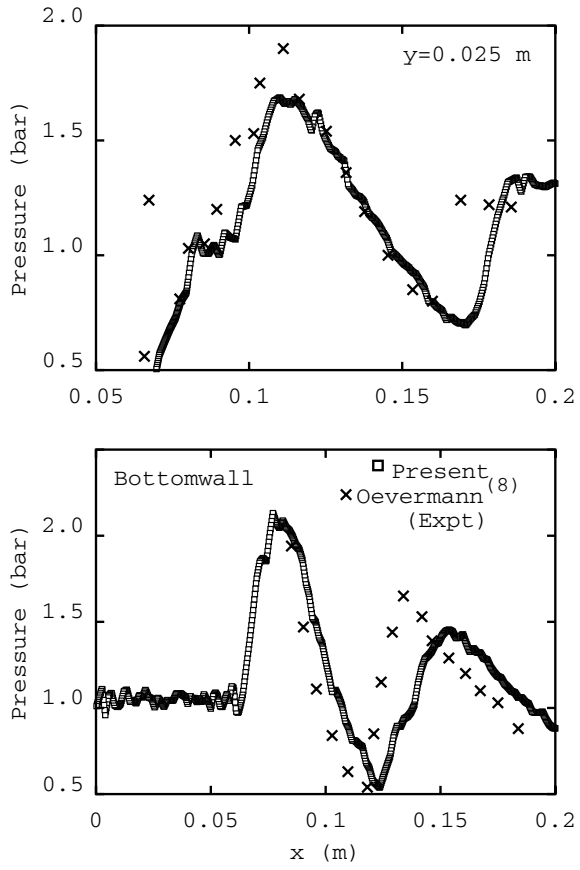


Figure 12. Static pressure distribution along y = 0·025m and along the bottom wall; non-reacting flow.

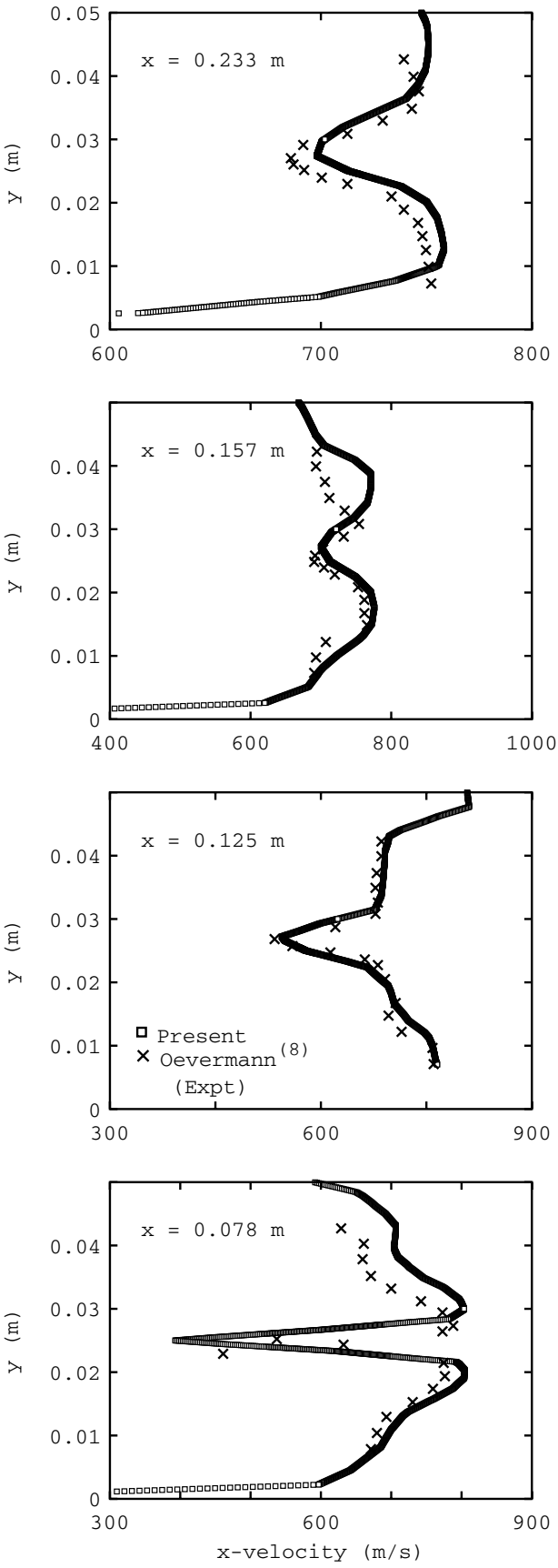


Figure 13. Variation of x-velocity at different x locations; non-reacting flow.

https://doi.org/10.1017/S0001924000001640 Published online by Cambridge University Press

Total pressure loss is defined as[11];

$$\eta_t = 1 - \frac{\int P_0 \rho u \mathrm{d}A}{\int P_{0,inlet} \rho u \mathrm{d}A}$$

The plot of η_t in Fig. 7. shows a gradual increase in the total pressure loss for $x > 0{\cdot}035$m due to the oblique shock from the leading edge of the wedge. This is followed by a sharp increase just beyond the trailing edge ($x = 0{\cdot}067$m) till about $x = 0{\cdot}1$m due to combustion and the accompanying heat release. This is consistent with the trend seen for combustion efficiency. There is a slight increase in total pressure loss beyond $x = 0{\cdot}1$ m, due to residual heat release as the combustion comes to a completion.

4.4 Comparison with experimental data

In this section, numerically predicted values of pressure, velocity, temperature and turbulent kinetic energy are compared with experimental values reported by Oevermann[8]. It should be borne in mind that the numerical results reported here are steady state results with fixed inlet conditions. In the experiments, small variations in the inlet conditions would have resulted in considerable variations in the location of shocks, separation, reattachment points as well as locations of heat release. Secondly, the adiabatic boundary conditions used in the simulations may not be realistic, as there would definitely have been heat transfer to the ambient during the experiments. Most importantly, the exact plane i.e., z = constant, where the measurements were taken was not reported by Oevermann[8]. It was mentioned that the measurements were taken near the side walls. In the absence of any quantitative information, in the following sub-sections, experimental data has been compared with numerical predictions on the symmetry plane, $z = 0{\cdot}025$m.

4.4.1 Non-reacting flow

Static pressure distribution along the bottom wall for the non-reacting flow case is given in Fig. 12. The initial pressure rise is due to the shock wave generated from the tip of the wedge. The decrease in pressure beyond $x = 0{\cdot}095$m is due to the expansion fan emanating from the base of the wedge as well as the diverging passage behind the wedge. The location and magnitude of the pressure peak due to the reflected shock wave beyond $x = 0{\cdot}125$m predicted by the calculations do not agree with the experimental data. Calculations predict the pressure peak to occur slightly downstream at $x = 0{\cdot}16$m compared with the experiments which show the peak to be at $x = 0{\cdot}13$m. The magnitude of the pressure rise is also underpredicted by the numerical calculations.

Static pressure distribution along the middle of the channel ($y = 0{\cdot}025$m) is also given in Fig. 12. The pressure initially increases in the separated region at the base of the wedge and then decreases due to the expansion in the diverging portion. The peak at $x = 0{\cdot}1$m is under-predicted by the calculations. However, the expansion between $0{\cdot}1 \le x \le 0{\cdot}16$m is predicted better. The sudden increase in pressure at $x = 0{\cdot}165$m due to the reflected shock wave is predicted to be somewhat downstream when compared with the experimental data. Variation of the x-velocity at $x = 0{\cdot}078$, $0{\cdot}125$, $0{\cdot}157$ and $0{\cdot}233$m is shown in Fig. 13. It is clear from this figure that the gradient based adaption procedure is able to capture the sharp variations in the velocity in the shear layer. The mixing and growth of the shear layer (as evidenced by the centreline velocity and the width of the jet) is also predicted reasonably by the numerical calculations. The maximum deviation between the prediction and the experiments is at $x = 0{\cdot}157$m and $y > 0{\cdot}03$m. As the mesh is fine in this region, the reason for this discrepancy is not clear. As the flow is not symmetric about the horizontal centreline, some degree of

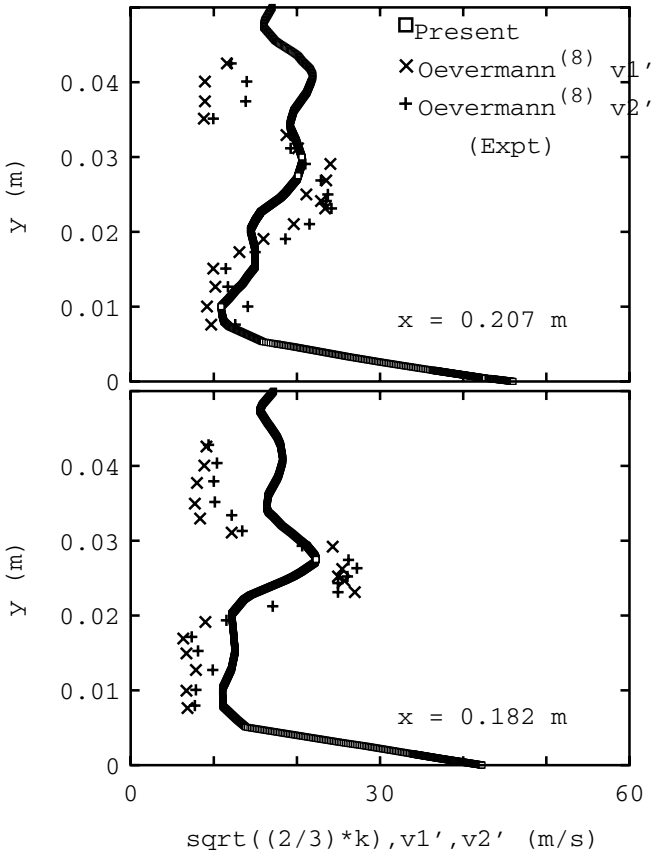


Figure 14. Variation of turbulent kinetic energy at different x locations; non-reacting flow.

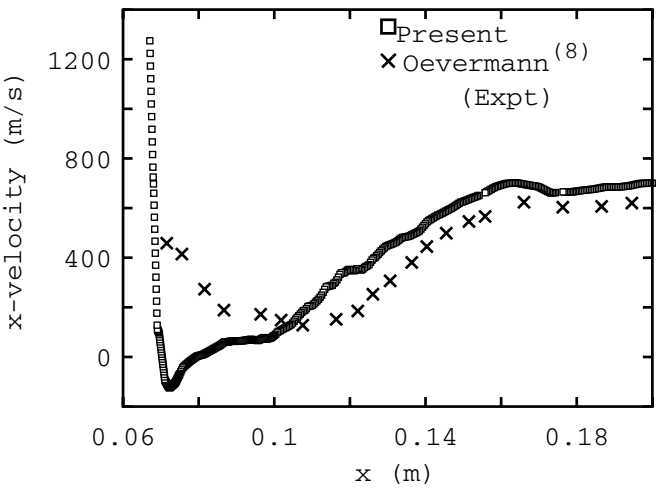


Figure 15. Variation of x-velocity along $y = 0{\cdot}025$m; reacting flow.

https://doi.org/10.1017/S0001924000001640 Published online by Cambridge University Press

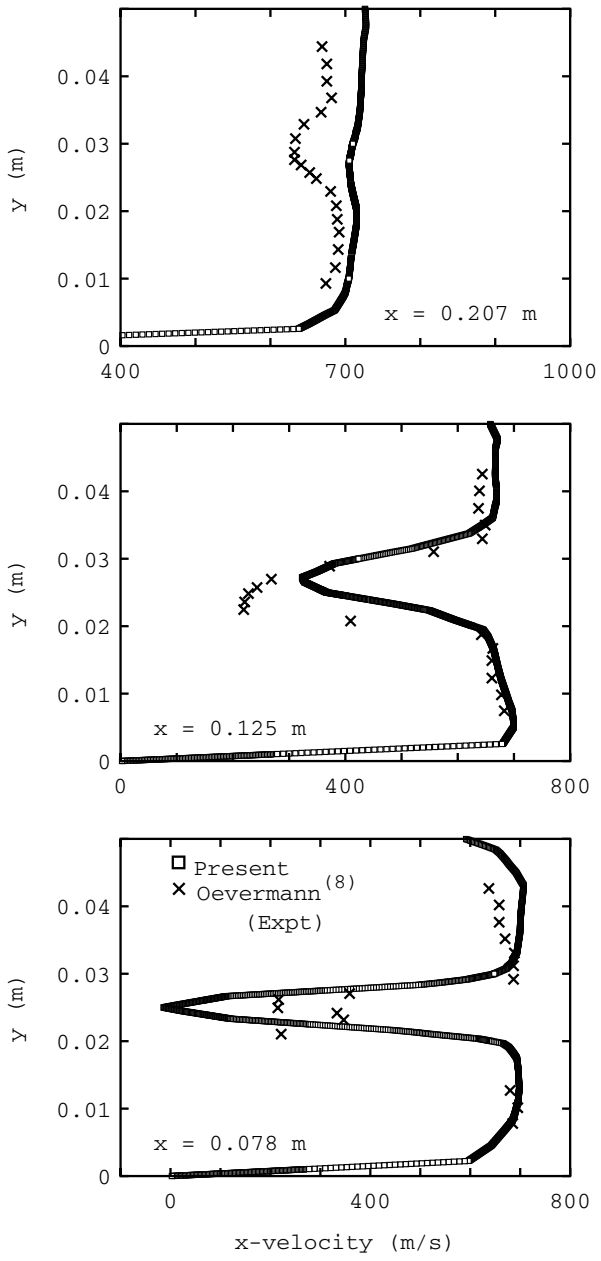


Figure 16. Variation of *x*-velocity at different *x* locations; reacting flow.

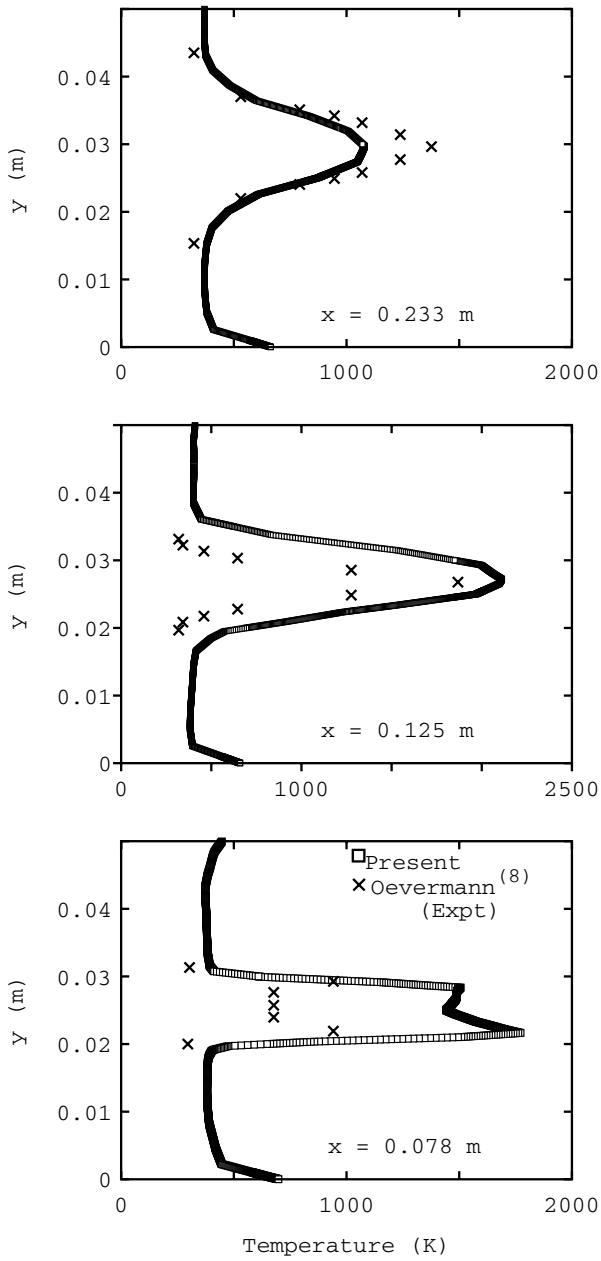


Figure 17. Variation of static temperature at different *x* locations; reacting flow.

asymmetry in the flow field is to be expected. However, the degree of asymmetry seen in the experimental data at $x = 0{\cdot}157$m might perhaps be due to unsteadiness in the flow.

A comparison of the turbulent velocity fluctuations from numerical calculations and from experimental measurements at $x = 0{\cdot}182$, $0{\cdot}207$m is given in Fig. 14. Since the numerical calculations are steady RANS calculations using k-ε model, velocity fluctuations have been calculated after assuming the turbulence to be isotropic, *viz*, $v' = \sqrt{2/3}k$. The experimental data also shows that u' and v' are almost equal, at least in the regions where measurements were made. It can be concluded from Fig. 14 that the numerical predictions are able to capture the trends reasonably well within the ambit of the realisable k-ε model. The agreement with the experimental data is better for the present 3D calculations than the 2D results reported by Oevermann[8].

4.4.2 Reacting flow

Variation of x-velocity along $y = 0{\cdot}025$m is given in Fig. 15. The agreement between the numerical prediction and the experimental data is not good in the region close to the point of injection (from $0{\cdot}07 \le x \le 0{\cdot}1$m) despite the fine resolution. The numerical data shows the presence of a subsonic recirculation region here whereas the experimental data does not show any such region. However, the agreement between the predictions and the experiment is better beyond $x = 0{\cdot}1$m. Variation of the x-velocity along the cross-stream direction at $x = 0{\cdot}078$, $0{\cdot}125$ and $0{\cdot}207$m is shown in Fig. 16. At all three x-locations, the agreement between the predictions and the experimental data is poor in the shear layer but it is better outside the shear layer. The disagreement at $x = 0{\cdot}078$m is especially severe as this is quite close to the injection port on the base of the ramp. Experimental data shows that the

https://doi.org/10.1017/S0001924000001640 Published online by Cambridge University Press

shear layer persists even at x = 0·207m but a shear layer is not discernable at this location in the numerical prediction.

Static temperature distribution shown in Fig. 17 also shows that the predictions are poor in the shear layer region. Numerical calculations grossly over-predict the temperature at x = 0·078m, show good agreement at x = 0·125m and grossly under-predict temperature at x = 0·233m. In other words, the temperature in the shear layer region predicted by the calculations is quite high even at x = 0·78m due to rapid combustion, whereas, at x = 0·233 m, the temperature is lower than the experimental value due to the expansion of the flow. The trends in Figs 16 and 17 show that the disagreement is primarily in the combustion zone. It can be concluded that the single step kinetics used in the present calculations predicts rapid combustion and heat release than what is seen in the experiment. This, in turn, affects the properties which are strong functions of temperature. Although combustion of H_2 is quite fast, with the equivalence ratio being so low in the present case, multi-step kinetics is certainly essential. This is evidenced by the fact that the temperatures predicted by the multi-step kinetics calculations of Oevermann[8] agree quite well with the experimental data. Turbulent velocity fluctuations from numerical calculations and from experimental measurements at x = 0·078, 0·125m and 0·157m is given in Fig. 18. In contrast to the non-reacting flow, the experimental data now shows considerable anisotropy in the shear layer especially close to the base of the wedge (x = 0·078m), but u' and v' are almost equal in other regions. Numerical predictions show good agreement with the experimental data in those regions where the turbulence is close to being isotropic, clearly bringing out the limitations of the k-ε model. As with the non-reacting flow case, the agreement with the experimental data is better for the present reacting, 3D calculations than the numerical results reported by Oevermann[8].

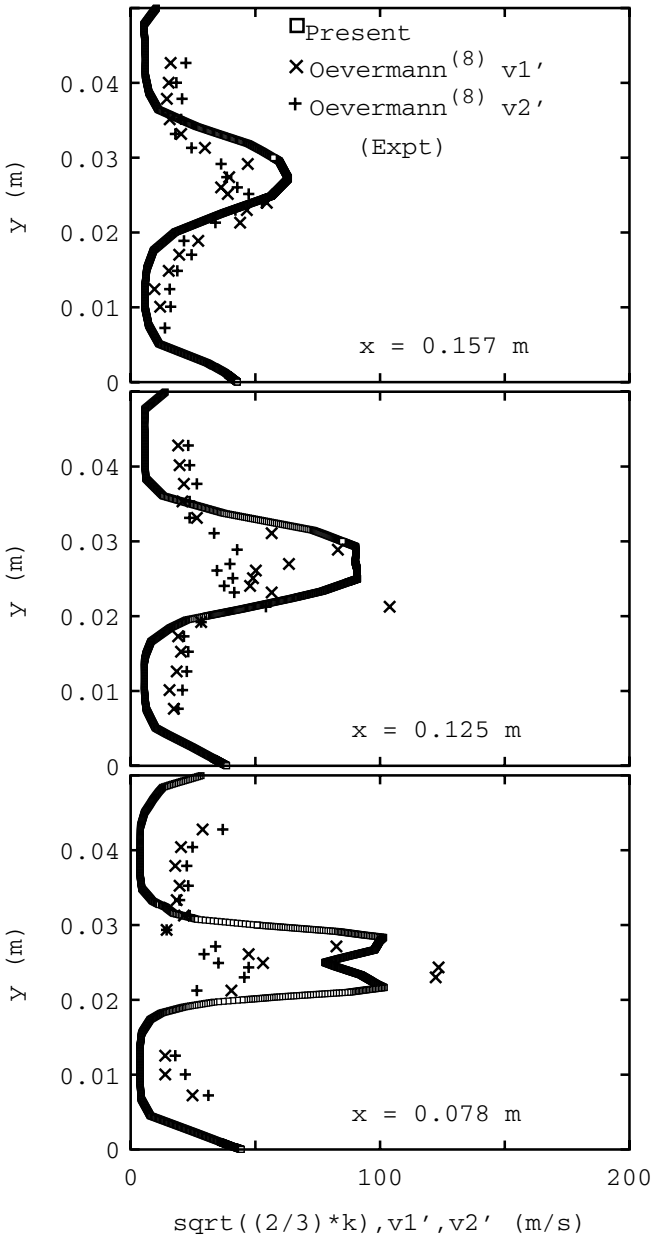


Figure 18. Variation of turbulent kinetic energy at different x locations; reacting flow.

5.0 SUMMARY AND CONCLUSIONS

Numerical simulation of 3D supersonic combustion using realisable k-ε turbulence model have been carried out. Single step reaction kinetics has been used for modelling the chemistry. Second order discretisation together with gradient based adaption and wall y+ refinement has been used to capture the intricate flow details. Area averaged wall y+ for the non-reacting and reacting flow results is 36. Comparison of the static pressure distribution on the bottom wall and middle section of the combustor and axial velocity variations at different x = constant locations show that the numerical predictions agree well with the experimental data. Calculated values for velocity fluctuations assuming isotropic turbulence agree reasonably well with experimentally measured velocity fluctuations. The k-ε model is able to predict the fluctuations well in those regions where the turbulence is reasonably isotropic. In strongly anisotropic regions such as the recirculation zone near the base of the wedge where combustion is taking place, there is considerable disagreement between the predictions and the experimental measurements.

Reacting flow calculations predict a temperature rise more rapid than what is seen in the experiments. Also, the disagreement between numerically predicted values for the x-velocity and the experimental data is severe in the recirculation region just downstream of the base of the wedge. These are most likely due to the single step chemistry model that is used in the calculations. The rapid heat release could also be due to over-prediction of the mixing rate. Calculations using multi step chemistry as well as different values for the turbulent Prandtl and Schmidt number should definitely be carried out to resolve these issues. In general, results from the present 3D calculations agree better with the experimental results than the 2D numerical results reported by Oevermann[8]. It can be concluded from the present work that RANS calculations on fine meshes with standard wall functions can predict the overall pressure rise and hence the thrust due to supersonic combustion reasonably well. However, use of these calculations for optimising injection and mixing strategies is still fraught with difficulties due to deficiencies in the turbulence models, as well as turbulence chemistry interaction. Xiao *et al*[12] have recently shown the importance of turbulence-chemistry interaction in such high speed flows. Measurements of the species concentrations inside the combustor will also help in better evaluating the current numerical models.

ACKNOWLEDGEMENTS

The authors would like to thank the reviewers for their comments and suggestions.

https://doi.org/10.1017/S0001924000001640 Published online by Cambridge University Press

REFERENCES

1. GOYNE, C.P., RODRIGUEZ, C.G., KRAUSS, R.H., MCDANIEL, J.C. and MCCLINTON, C.R. Experimental and numerical study of dual mode scramjet combustor, 2002, AIAA paper 2002-5216.
2. KIM, J.H., YOON, Y., JEUNG, I.S., HUH, H. and CHOI, J.Y. Numerical study of mixing enhancement by shock waves in a model scramjet engine, *AIAA J*, 2003, **41**, (6).
3. KIM, K.M., BAEK, S.W. and HAN, C.Y. Numerical study on supersonic combustion with cavity based fuel injection, *Int J Heat and Mass transfer*, 2004, **47**, pp 271-286.
4. RODRIGUEZ, C.G., WHITE, J.A. and RIGGINS, D.W. Three-dimensional effects in modelling of dual mode scramjets, 2000, AIAA paper 2000-3704.
5. RODRIGUEZ, C.G. and CUTLER, A.D. Numerical analysis of the SCHOLAR supersonic combustor, NASA-CR-2003-212689, 2003.
6. BAURLE, R.A. Modelling of high speed reacting flows: Established Practices and Future Challenges, 2004, AIAA paper 2004-0267.
7. RAJASEKARAN, A. and BABU, V. Numerical simulation of three-dimensional reacting flow in a model supersonic combustor, *J Propulsion and Power*, 2006, **22**, (4), pp 820-827.
8. OEVERMANN M. Numerical investigation of turbulent hydrogen combustion in a SCRAMJET using flamelet modeling, *Aerospace Science and Technology*, 2000, **4**, pp 463-480.
9. BAURLE R.A. and EKLUND D.R. Analysis of dual-mode hydrocarbon scramjet operation at Mach 4-6.5, *J Propulsion and Power*, 2002, **18**, (5), pp 990-1002.
10. HSU, K. and JEMCOV, A. numerical investigation of detonation in pre-mixed H_2-Air mixture-Assessment of simplified chemical mechanism, 2000, AIAA paper 2000-2478.
11. BAURLE, R.A., MATHUR, T., GRUBER, M.R. and JACKSON, K.R. A numerical and experimental investigation of a scramjet combustor for hypersonic missile applications, 1998, AIAA paper 98-3121.
12. XIAO X., HASSAN H.A. and BAURLE R.A. Modelling scramjet flows with variable turbulent Prandtl and Schmidt Numbers, 2006, AIAA paper 2006-128.

https://doi.org/10.1017/S0001924000001640 Published online by Cambridge University Press